
Good Actors can come in Smaller Sizes: A Case Study on the Value of Actor-Critic Asymmetry

Siddharth Mysore¹ Bassell Mabsout¹ Renato Mancuso¹ Kate Saenko^{1,2}

Abstract

Actors and critics in actor-critic reinforcement learning algorithms are functionally separate, yet they often use the same network architectures. This case study explores the performance impact of network sizes when considering actor and critic architectures independently. By relaxing the assumption of architectural symmetry, it is often possible for smaller actors to achieve comparable policy performance to their symmetric counterparts. Our experiments show up to 97% reduction in the number of network weights with an average reduction of 64% over multiple algorithms on multiple tasks. Given the practical benefits of reducing actor complexity, we believe configurations of actors and critics are aspects of actor-critic design that deserve to be considered independently.

1. Introduction

Actor-critic methods are currently amongst the most common class of model-free deep reinforcement learning (RL) algorithms. They are characterized by their separation of the functions representing the actor — the RL policy — and the critic — the value function estimator. This allows actor-critic methods to theoretically take advantage of the improved sample efficiency of value-based RL approaches like Q-learning (Watkins & Dayan, 1992) while also capitalizing on the ability to use policy-based approaches such as policy gradient (Sutton et al., 2000), enabling learning on continuous action domains and improved robustness to stochasticity. Actor-critic methods are also widely represented in common baselines and benchmarks (Dhariwal et al., 2017; Hill et al., 2018; Raffin et al., 2019; Brockman et al., 2016; Raffin et al., 2019; Guadarrama et al., 2018), making them an attractive foundation upon which to develop new research and technologies.

¹Department of Computer Science, Boston University, Boston, MA, USA ²MIT-IBM Watson AI Lab. Correspondence to: Siddharth Mysore <sidmys@bu.edu>.

The separation of actors and critics means that only the actor is required during inference. This can be critically advantageous in compute-constrained applications as it spares the expense estimation policy value, which mainly useful only during training. Beyond excluding the critic, further reducing run-time compute requires reducing actor sizes, leading us to ask how small actors can get before losing learning efficacy. Works considering the impact of network architectures on RL performance typically adjust both actor and critic sizes equivalently (Pineau et al., 2020; Zhang et al., 2018b;a; Islam et al., 2017; Duan et al., 2016), i.e. their architectures are kept ‘symmetric’. Nonetheless, nothing in the theoretical foundations precludes using different architectures for actors and critics. In this work, we study if symmetry is important to actor-critic methods and how relaxing the self-imposed symmetry impacts performance and model complexity. We find this actor-critic ‘asymmetry’ allows for a significant reduction in actor network sizes without compromising the algorithms’ performances.

Our contributions: With this case study, we explore how disentangling actor and critic architectures’ can impact learning and run-time performance. We test 4 popular actor-critic algorithms on 6 different environments of varying system dynamics. We show that it is not simply that network architectures often presented in contemporary literature have a lot of headroom with model complexity but that actors require less modeling capacity than critics, allowing them to function with smaller architectures. The practical implications of this intuitive observation have received little attention, and no prior study has been conducted to systematically understand and evaluate the potential of asymmetry in actor-critic methods. Our results show that asymmetry enables reductions in actor sizes of up to 97% even over actors that have already been shrunk through symmetric architecture tuning. We hypothesize that modeling the value function associated with an environment often requires a higher capacity for modeling complexity. This is because the critic needs to develop an understanding of both the dynamics of a black-box system and how they contribute to learning rewards. Actors try to maximize the value estimate, which is done by gradient ascent on the value function estimate. Evidence suggests this is often easier to optimize, requiring less modeling complexity, allowing for smaller actors.

2. Background and Related Work

Actor-critic methods separate the actor and critic functions of an RL algorithm. The actor function represents the policy, i.e. the core of the decision making aspect of the RL algorithm, while the critic estimates the value of trajectories of state transitions under the policy. Actor-critic algorithms are typically trained through sampling based value iteration and policy gradients, where critics are trained to minimize the loss on the measured returns against the estimated value and actors are trained to maximize the estimated value of the trajectories generated under the actor policy. Specifics of how the optimization criteria are estimated can vary between algorithms. Prominent contemporary algorithms under the actor-critic umbrella include A2C (Mnih et al., 2016), A3C (Shen et al., 2020), PPO (Schulman et al., 2017), TRPO (Schulman et al., 2015), DDPG (Lillicrap et al., 2016), TD3 (Fujimoto et al., 2018), and SAC (Haarnoja et al., 2018), to name a few.

An increasingly wide corpus of studies focused on the reproducibility of RL algorithms have shown them to be highly sensitive to implementation details and hyper-parameters (Pineau et al., 2020; Henderson et al., 2018; Zhang et al., 2018b;a; Islam et al., 2017; Duan et al., 2016). Network architecture is one of many hyper-parameters that can impact actor-critic performance (Henderson et al., 2018; Islam et al., 2017; Zahavy et al., 2020; Zhang et al., 2018b). Islam et al. (2017) and Zahavy et al. (2020) address the importance of network sizes and architectures but do not consider actors' and critics' architectures separately. We believe, however, that this is an important consideration to make, but one that is easily missed given that tools most commonly available typically hard-code actor/critic symmetry. Indeed, by surveying existing baseline codes including OpenAI Baselines (Dhariwal et al., 2017), OpenAI Spinning Up (Achiam, 2018), Stable Baselines (v2 and v3) (Hill et al., 2018; Raffin et al., 2019), Tensorflow RL Agents (Guadarrama et al., 2018), and rllab (Duan et al., 2016), we found that actor and critic architectures are generally entangled and symmetric — in most cases allowing users to define an architecture for both the actor and critic networks together but not independently.

Henderson et al. (2018) provide a cursory analysis on the impact of disentangling the actor and critic architectures and consider how different algorithms behave in different training environments as a result of changing network structures. They note the sensitivity of algorithms to these details but a limitation of their analysis is that it sacrifices depth for breadth as this is just one of many hyper-parameters they investigate. Their analysis appears to primarily seek to identify if there is a correlation between performance and actor and critic architectures when considered independently. However only two environments and a limited set of net-

work configurations are tested, preventing clear conclusions being drawn on *how* actor and critic architectures relate to each other. By considering a wider range of network sizes and environments, we are able to formulate and test a clearer hypothesis on the relationship between network sizes, both for the actors and critics, and their impact on performance.

Reducing the parameter count of neural networks has also received interest in the broader machine learning community. Techniques like pruning (Han et al., 2016), knowledge distillation (Hinton et al., 2015), and weight sharing (Ullrich et al., 2017) have been shown to accelerate inference and reduce memory requirements, enabling deployment on resource-constrained mobile hardware. In RL, policy distillation (Rusu et al., 2015) has been demonstrated as an effective tool for reducing network sizes using a teacher-student method where a larger pre-trained teacher network guides a smaller student network which learns to match the teacher's performance. Smaller students learning equivalently functional policies hints at an excess in modeling capacity of the policy networks, prompting investigation on whether initial training can yield smaller viable actors.

3. Motivating Example: A Toy Problem

We start with a toy-problem that we know could be solved, in principle, by a very small (1-neuron) actor. We constructed a simple one-dimensional goal-tracking problem without complex dynamics or system noise. The agent's observed state o is the difference between the desired goal g and current internal state s , $o = g - s$, where $s, g \in [-1, 1]$. Actions a affect the internal state such that the next state $s' = s + a$. This problem is solved completely with the ideal policy $a^* = o$, and is solvable by a single neuron that returns the input as output.

We considered every algorithm included in the OpenAI Spinning Up code-base (Achiam, 2018), which includes TRPO, PPO, DDPG, SAC and TD3. The code-base, by default, allows users to jointly adjust the number of hidden layers and the number of hidden neurons per layer in the actor and critic networks. For all algorithms tested however, when trained with the implicit assumption of actor and critic network symmetry, it was not possible for agents to learn to solve even this simple problem with a 1-neuron policy. We will note however that it is possible for the single neuron weight to be randomly initialized close to 1, which effectively solves the problem, though does not count as a learned solution. We tested network architectures including $|1|$, $|4, 4, 1|$, $|8, 8, 1|$ and $|16, 16, 1|$, where numbers within the vertical brackets provide a comma-delimited representation of the number of neurons per layer in the neural network, with the last layer being the 1-D output. When structured symmetrically, we found that agents did not consistently train to solve this problem below the $|8, 8, 1|$ structure but were most stable

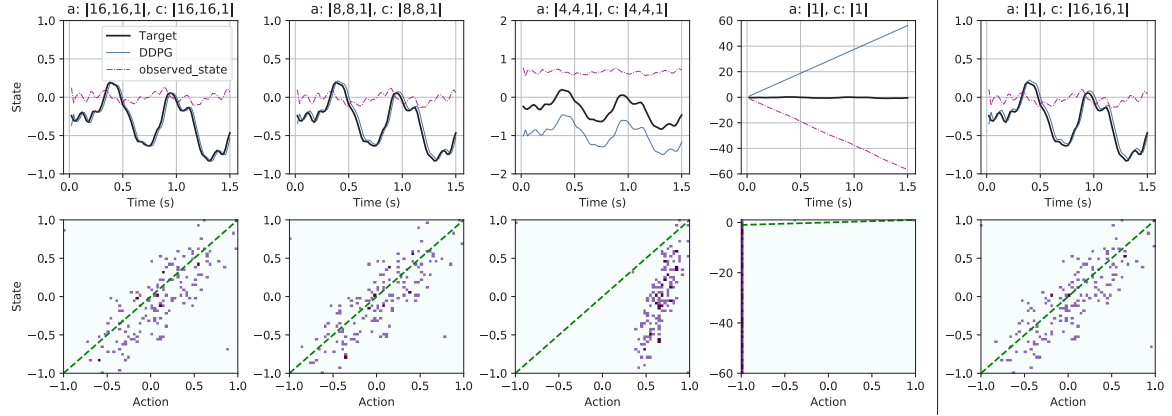


Figure 1. State transitions and state-action distributions for different actor [a] and critic [c] sizes. This visualizes their ability or lack thereof to solve this simple tracking problem. The green dotted line in the state-action plots represents the ideal action policy. With a larger critic, the 1-neuron actor (right) is able to perform similarly to an actor several times larger that shares the same critic size (left). Crucially, this shows that with sufficient modeling capacity in the critic, a single neuron indeed learns to solve this simple problem.

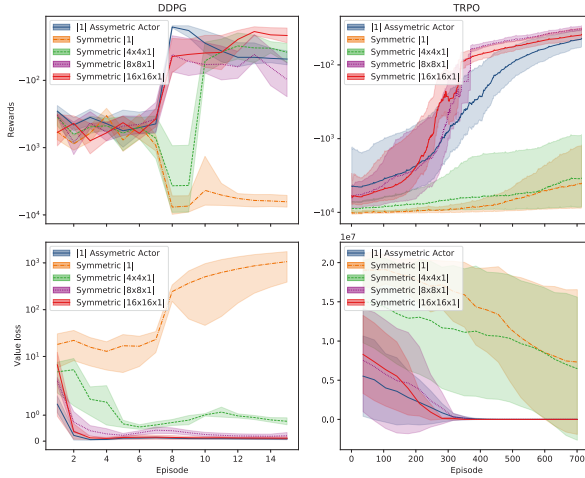


Figure 2. Comparison of how rewards and value (critic) losses evolve during training on a simple toy-problem. Results suggest a strong correlation between critic size and policy viability. Symmetric policies share the same size as their critics while the asymmetric actor has a 1-neuron policy and a $|16, 16, 1|$ critic. Note that the asymmetric actor performs very similarly to the symmetric $|16, 16, 1|$ policy and shares a similar value loss profile too.

with $|16, 16, 1|$. Figure 2 shows training trends for agents trained with DDPG and TRPO on this problem (see Figure A.1 for SAC, TD3 and PPO). Figure 1 compares the quality of learned control. Note that a 1-neuron actor is not capable of learning to solve this problem when paired with a 1-neuron critic, but learns viable policies when trained with a larger critic. Trends in rewards and losses during training indicated that an improvement in value estimation was followed shortly thereafter by an improvement in the observed rewards. We hypothesized that it was the smaller critics that were lacking in their ability to model the underlying value functions. To test this, we restricted the actor size to be 1-neuron and set the critic to be $|16, 16, 1|$. By breaking from the implicit assumption of actor-critic symmetry and

separately considering the actor and critic architecture, it was possible to consistently train 1-neuron actors where the smaller symmetrically sized 1-neuron critics had failed. Figures 2 and 1 demonstrate that, in addition to allowing for successful training, the asymmetric model shares similar training and loss optimization characteristics to its larger symmetric counterpart.

4. Benchmarking Asymmetric Actors

It was evident that separately defining actor and critic architectures was at least helpful in the case of a simple toy problem. To better understand the practical implications of actor-critic asymmetry, we evaluated how different network sizes affect performance on a number of common benchmark tasks from OpenAI’s Gym (Brockman et al., 2016) benchmark environments. Prior work by Islam et al. (2017) and Henderson et al. (2018) touch on the impact of network size on the performance of RL algorithms but their analyses are more limited to a smaller set of environments and architectures. Both works consider networks with 3 different possible hidden layer configurations: $|400, 300|$, $|64, 64|$ and $|100, 50, 25|$, common sizes used in prior literature. There is anecdotal evidence in these works to suggest that larger actors are not necessarily better and that larger critics can usually perform better, but the data presented does not lend itself to clear conclusions.

To better characterize how network size can affect performance, and specifically how smaller networks impact performance, we consider two aspects of the actor-critic architecture: (i) the smallest symmetric actor-critic architecture that can meaningfully solve the problem, and similarly (ii) the smallest asymmetric architecture with comparable performance. Treating $|400, 300|$ as the upper bound on a set of possible 2-hidden-layer architectures, we consider the structures: $|1, 1|$, $|4, 4|$, $|8, 8|$, $|16, 16|$, $|32, 32|$, $|64, 64|$,

Table 1. Exploring the impact of actor-critic asymmetry on algorithm performance (improvements in size are in **bold**)

Algorithm	Threshold	Size	Baseline		Symmetric Actor		Asymmetric Actor		
			Reward	Size ↓	Reward ↑	Actor Size ↓	Reduction ↑	Critic Size	Reward ↑
Pendulum-v0									
DDPG	-160	[400, 300]	-145.56 ± 10.64	[16, 16]	-150.28 ± 9.08	[4, 4]	88.38%	[16, 16]	-158.97 ± 5.33
TD3	-160	[400, 300]	-152.71 ± 9.47	[16, 16]	-152.42 ± 6.65	[4, 4]	88.38%	[16, 16]	-167.57 ± 14.53
SAC	-160	[256, 256]	-139.86 ± 8.29	[16, 16]	-155.32 ± 11.25	[4, 4]	88.38%	[16, 16]	-153.86 ± 10.97
PPO	-200	[64, 64]	-668.60 ± 551.85	[128, 128]	-193.55 ± 40.14	[128, 128]	0%	[128, 128]	-193.55 ± 40.14
Reacher-v2									
DDPG	-6.0	[400, 300]	-4.26 ± 0.25	[64, 64]	-4.75 ± 0.19	[8, 8]	96.33%	[64, 64]	-4.80 ± 0.44
TD3	-7.0	[400, 300]	-6.52 ± 1.12	[64, 64]	-6.91 ± 0.74	[32, 32]	70.23%	[64, 64]	-6.68 ± 1.21
SAC	-6.5	[256, 256]	-5.96 ± 0.47	[128, 128]	-6.05 ± 0.91	[16, 16]	97.28%	[128, 128]	-6.02 ± 1.07
PPO	-5.5	[64, 64]	-4.37 ± 1.74	[64, 64]	-4.37 ± 1.74	[16, 16]	90.15%	[64, 64]	-5.49 ± 1.00
Ant-v2									
DDPG	-	[400, 300]	225.23 ± 362.88	-	-	-	-	-	-
TD3	3000	[400, 300]	3087.86 ± 888.75	[256, 256]	3944.78 ± 745.48	[32, 32]	94.92%	[256, 256]	3553.52 ± 396.30
SAC	3000	[256, 256]	3366.07 ± 1522.45	[64, 64]	3108.63 ± 519.59	[64, 64]	0%	[64, 64]	3108.63 ± 519.59
PPO	3000	[64, 64]	3734.58 ± 988.29	[8, 8]	3723.57 ± 760.94	[8, 8]	0%	[8, 8]	3723.57 ± 760.94
HalfCheetah-v2									
DDPG	7000	[400, 300]	7026.01 ± 202.78	[64, 64]	7450.01 ± 950.15	[32, 32]	68.01%	[64, 64]	8273.76 ± 437.66
TD3	8000	[400, 300]	8861.92 ± 870.02	[64, 64]	8315.13 ± 262.78	[32, 32]	68.01%	[64, 64]	8145.84 ± 262.55
SAC	10000	[256, 256]	11554.76 ± 779.91	[64, 64]	10180 ± 759.10	[32, 32]	68.01%	[64, 64]	9619 ± 158.40
PPO	3000	[64, 64]	3395 ± 1156.30	[64, 64]	3395 ± 1156.30	[32, 32]	68.01%	[64, 64]	3089 ± 919.25
Acrobot-v1									
SAC	-100	[256, 256]	-76.5 ± 4.30	[32, 32]	-86.5 ± 7.54	[16, 16]	68.46%	[32, 32]	-90.5 ± 8.12
PPO	-100	[64, 64]	-74.7 ± 0.30	[8, 8]	-70.75 ± 0.33	[1, 1]	90.33%	[8, 8]	-71.75 ± 0.50

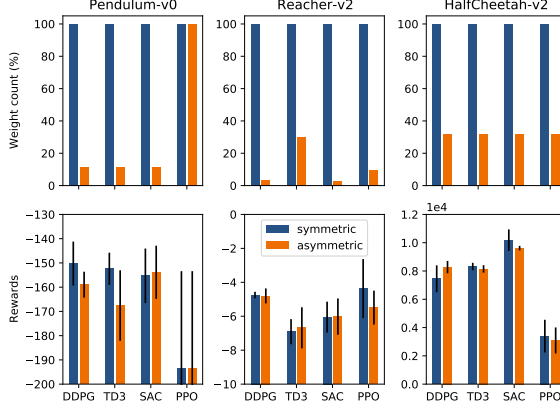


Figure 3. Comparing the relative actor network sizes (as functions of the number of network weights) and rewards for the smallest actors found through a binary search on symmetrically constrained vs. the asymmetric, unconstrained actors. Results evidence that it is often possible to train significantly smaller actors with larger critics without compromising performance.

$[128, 128]$, $[256, 256]$ and $[400, 300]$. This list covers typical architectures found in actor-critic literature but also goes smaller to get a sense the lower bound on the network complexity needed for the considered tasks.

Experimental Method: We determine appropriate sizes for the smallest symmetric and asymmetric architectures sequentially. By running the algorithms on 6 random seeds with their originally reported architectures, we establish a baseline and a threshold target performance for smaller networks. We then use this threshold with a 10% tolerance to find with a binary search the actor-critic networks that can solve the problem while preserving actor-critic symmetry, while similarly averaging performance over 6 seeds. Finally, by locking the critic architecture to the smallest symmetric

size found, we repeat the binary search over the possible actor architectures to find the smallest asymmetric actor that would solve the problem. This allows us to determine more conclusively that, in cases where asymmetry allows for actor size reduction, it is not simply attributable to excess modeling capacity in both the actor and critic networks.

Our results are shown in Table 1, covering 4 algorithms: DDPG (Lillicrap et al., 2016), TD3 (Fujimoto et al., 2018), SAC (Haarnoja et al., 2018) and PPO (Schulman et al., 2017). With the exception of PPO, we used codes provided by the OpenAI Spinning Up (Achiam, 2018) code-base, with training hyper-parameters from the RL-zoo (Hill et al., 2018). As shown by Engstrom et al. (2020) and Ilyas et al. (2020) PPO can be highly sensitive to implementation details, so we instead used the OpenAI Baselines (Dhariwal et al., 2017) implementation of PPO to maintain parity with the original work. In an effort to cover a wide range of possible system dynamics, these algorithms were tested on 5 environments: Pendulum-v0, Reacher-v2, Ant-v2¹, HalfCheetah-v2 and Acrobot-v1². Asymmetry has demonstrable utility in reducing actor sizes in every environment tested. Though it is possible for the automated search to find actors larger than their critics, such a case did not arise in testing. Gains vary by algorithm and environment, with between 70–97% actor size reductions, and with the Q-learning based algorithms (DDPG, TD3 and SAC) sharing similar trends. PPO appears to be more unpredictable in performance, particularly when considering the disparities in network size to performance over Pendulum-v0, Ant-v2 and Acrobot-v1. Despite poor performance on the simple

¹Due to DDPG being incapable of reasonably solving the Ant task in our experiments, it is omitted for the Ant-v2 environment.

²Acrobot-v1 is a discrete action-space environment thus restricting DDPG and TD3 which were coded for continuous control.

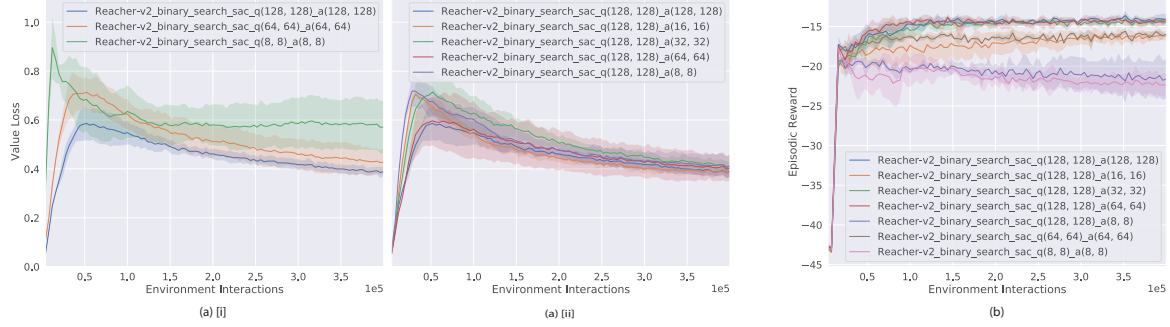


Figure 4. Training progress for SAC on Reacher-v2: (a) Q-Value Loss during training and (b) the episodic returns. (a)[i] Shows the value loss during training for different critic sizes while (a)[ii] shows the same for different actors trained with the same critic size. Changing the critic’s size impacts value-loss more than changing the actor’s, suggesting that the critic is more sensitive to changes in modeling capacity.

inverted pendulum problem with smaller networks where other algorithms succeed, PPO solves the more complicated multi-pedal locomotion problem in Ant-v2 with significantly smaller actor and critic networks compared to the other algorithms tested and is similarly able to solve the Acrobot-v1 problem with smaller networks than SAC. It does however present with actor size reduction through asymmetry in 3 out of 5 environments.

To further illustrate the significance of these values, we also show in Figure 3 a comparison of the relative differences in network sizes as well as the rewards achieved by the smallest symmetrically constrained and asymmetric actors for the Pendulum-v0, Reacher-v2 and HalfCheetah-v2 tasks. In the most dramatic reductions, we can observe size reductions in excess of 95% over the already symmetrically size-reduced actors on the Reacher-v2 task with DDPG and SAC with no significant impact on the rewards achieved.

Experimental observations also provide empirical validation of our hypothesis that modeling capacity in the critic is often the limiting factor in achieving successful training. This is best illustrated by data on the training of SAC on the Reacher-v2 task and is shown in Figure 4 where there are relatively clear demarcations in where the Q-value losses and episodic rewards saturate for different network sizes. While changing the size of the critic during the symmetric binary search has a noticeable impact on the Q-value loss, changing the actor size during asymmetric search does not impact the Q-value loss significantly, as shown when comparing Figures 4(a)[i] and [ii]. A larger critic also allows for a much smaller actor to be successfully trained (in this case a critic with hidden layers of size [128, 128] allows for an actor of size [16, 16]). We can therefore draw the conclusion that the dominant limiting factor in learning, for this algorithm, on this environment, is indeed the modeling capacity of the critic. Similar trends can be observed for other algorithms in other training tasks too, the visualizations for which are provided in Appendix B. Training codes for all experiments discussed in this paper are also available at <https://tinyurl.com/AsymmetricAC-Code>.

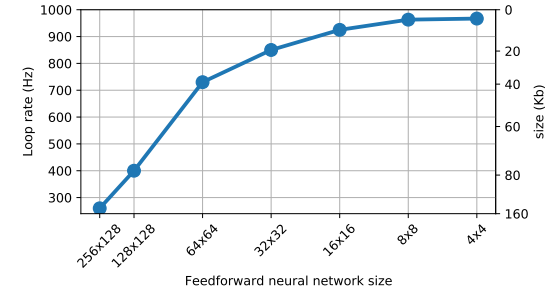


Figure 5. Comparison of feed-forward inference rates for networks of different sizes on an STM32F722RE micro-controller. Larger networks significantly impact the loop rate, which is highly detrimental to control sensitivity and functionality.

5. The Value of Smaller Actors

Networks typically used in feed-forward RL are not ‘large’ in the conventional sense, particularly when compared to deep networks in other fields of machine learning and artificial intelligence, so it would be natural to question why these results are significant. One of the most common practical use-cases for RL is in control systems — such as locomotion control in various robotic systems (Sadeghi et al., 2017; Molchanov et al., 2019; Andrychowicz et al., 2020; Mahmood et al., 2018; Mysore et al., 2020a;b; Koch et al., 2018). Mobile platforms, particularly, are often constructed with resource constraints in mind, where networks that may be regarded as ‘small’ in other use cases can still exceed the platforms’ operational capacity.

Consider for example the STM32F722RE micro-controller which has notably been used in aerobatic high-performance drone flight-controllers such as the Matek F722-STD ([Mateksys](#)). When employing a classical controller such as a PID-controller, the platform operates at a 1kHz loop-rate. When deploying neural-network based controllers however, despite compiling the graphs with optimizations enabled for the target hardware, there are two major limitations: (i) control firmware needs to fit into 181kB of available memory, however large networks consume too much memory, and (ii) even if a network can fit in

memory, the compute required to evaluate the forward pass of a larger network can significantly impact inference speed. Figure 5 highlights the relationship between network size and memory requirements and control rate. Even a network with hidden layer structure $[128, 128]$ can reduce inference from the target 1kHz to 400Hz, severely limiting responsiveness and functionality of the platform. At $[256, 128]$, the network is near the memory capacity of the controller and operates at approximately 250Hz, though with high variance and intermittent failure to respond to external control signals, making it risky to operate. Larger networks, including $[256, 256]$ and above (which we note is still smaller than the $[400, 300]$ network size typically reported for DDPG and TD3) would simply not fit within available memory.

Even in larger systems, with a higher compute and memory budget, smaller memory footprints allow for better cache locality making tasks less prone to interference (Bechtel et al., 2018). Similarly, resource savings from smaller networks for controls tasks can also be useful when deploying multiple networks simultaneously, for example in a multi-agent setting. It is important to preserve operational stability and consistency, particularly in real-time systems where hiccups can result in catastrophic failure and smaller networks with their lower resource costs afford systems more redundancy.

6. Conclusion

We hypothesized that this capacity for actor size reduction comes from the burden of modeling and understanding environment dynamics falling largely to the critic, rather than the actor. Provided that the critic has sufficient capacity to learn a decent estimation of the value function, we predicted that it would often be possible to train actors that are significantly smaller than the critic. The results presented in this case study substantiate this hypothesis. We demonstrated that, by relaxing the implicit assumption of symmetry in the architectures of actors and critics in actor-critic RL, it is possible to train significantly smaller networks for tasks without a significant degradation in policy performance. We demonstrate as much as a 97% reduction in the number of weights needed to represent viable actor policies, with an average actor size reduction of 63.60% in actor network sizes for the tested tasks. We believe that the implications of these results can be highly significant to practical applications of RL, particularly in resource-constrained systems, and that it is also worth being generally aware of as part of the broader effort to understand how network sizes can impact actor-critic RL performance.

References

Python noise library version 1.2.3. URL <https://github.com/caseman/noise/tree/bb32991ab97e90882d0e46e578060717c5b90dc5>. Accessed: 2021-02-04.

Achiam, J. Spinning Up in Deep Reinforcement Learning. 2018.

Andrychowicz, O. M., Baker, B., Chociej, M., Józefowicz, R., McGrew, B., Pachocki, J., Petron, A., Plappert, M., Powell, G., Ray, A., Schneider, J., Sidor, S., Tobin, J., Welinder, P., Weng, L., and Zaremba, W. Learning dexterous in-hand manipulation. *The International Journal of Robotics Research*, 39(1):3–20, 2020. doi: 10.1177/0278364919887447. URL <https://doi.org/10.1177/0278364919887447>.

Bechtel, M. G., McEllhiney, E., Kim, M., and Yun, H. Deep-picar: A low-cost deep neural network-based autonomous car. In *2018 IEEE 24th International Conference on Embedded and Real-Time Computing Systems and Applications (RTCSA)*, pp. 11–21. IEEE, 2018.

Brockman, G., Cheung, V., Pettersson, L., Schneider, J., Schulman, J., Tang, J., and Zaremba, W. Openai gym. *CoRR*, abs/1606.01540, 2016.

Dhariwal, P., Hesse, C., Klimov, O., Nichol, A., Plappert, M., Radford, A., Schulman, J., Sidor, S., Wu, Y., and Zhokhov, P. Openai baselines. <https://github.com/openai/baselines>, 2017.

Duan, Y., Chen, X., Houthooft, R., Schulman, J., and Abbeel, P. Benchmarking deep reinforcement learning for continuous control. In *Proceedings of the 33rd International Conference on International Conference on Machine Learning - Volume 48*, ICML’16, pp. 1329–1338. JMLR.org, 2016.

Engstrom, L., Ilyas, A., Santurkar, S., Tsipras, D., Janoos, F., Rudolph, L., and Madry, A. Implementation matters in deep rl: A case study on ppo and trpo. In *International Conference on Learning Representations*, 2020.

Fujimoto, S., Hoof, H., and Meger, D. Addressing function approximation error in actor-critic methods. In *International Conference on Machine Learning*, pp. 1587–1596, 2018.

Guadarrama, S., Korattikara, A., Ramirez, O., Castro, P., Holly, E., Fishman, S., Wang, K., Gonina, E., Wu, N., Kokiopoulou, E., Sbaiz, L., Smith, J., Bartók, G., Berent, J., Harris, C., Vanhoucke, V., and Brevdo, E. TF-Agents: A library for reinforcement learning in tensorflow. <https://github.com/tensorflow/agents>, 2018. URL <https://github.com/tensorflow/agents>.

`tensorflow/agents`. [Online; accessed 25-June-2019].

Haarnoja, T., Zhou, A., Abbeel, P., and Levine, S. Soft actor-critic: Off-policy maximum entropy deep reinforcement learning with a stochastic actor. *International Conference on Machine Learning (ICML)*, 2018.

Han, S., Mao, H., and Dally, W. Deep compression: Compressing deep neural network with pruning, trained quantization and huffman coding. *arXiv: Computer Vision and Pattern Recognition*, 2016.

Henderson, P., Islam, R., Bachman, P., Pineau, J., Precup, D., and Meger, D. Deep reinforcement learning that matters. In *Proceedings of the AAAI Conference on Artificial Intelligence*, volume 32, 2018.

Hill, A., Raffin, A., Ernestus, M., Gleave, A., Kanervisto, A., Traore, R., Dhariwal, P., Hesse, C., Klimov, O., Nichol, A., Plappert, M., Radford, A., Schulman, J., Sidor, S., and Wu, Y. Stable baselines, 2018.

Hinton, G. E., Vinyals, O., and Dean, J. Distilling the knowledge in a neural network. *ArXiv*, abs/1503.02531, 2015.

Ilyas, A., Engstrom, L., Santurkar, S., Tsipras, D., Janoos, F., Rudolph, L., and Madry, A. A closer look at deep policy gradients. In *International Conference on Learning Representations*, 2020.

Islam, R., Henderson, P., Gomrokchi, M., and Precup, D. Reproducibility of benchmarked deep reinforcement learning tasks for continuous control. *arXiv preprint arXiv:1708.04133*, 2017.

Koch, W., Mancuso, R., West, R., and Bestavros, A. Reinforcement learning for UAV attitude control. *ACM Transactions on Cyber-Physical Systems*, 2018.

Lillicrap, T. P., Hunt, J. J., Pritzel, A., Heess, N., Erez, T., Tassa, Y., Silver, D., and Wierstra, D. Continuous control with deep reinforcement learning. *International Conference on Learning Representations*, 2016.

Mahmood, A. R., Korenkevych, D., Vasan, G., Ma, W., and Bergstra, J. Benchmarking reinforcement learning algorithms on real-world robots. *Conference on Robot Learning*, 2018. URL <http://arxiv.org/abs/1809.07731>.

Mateksys. Flight controller f722-std. <http://www.mateksys.com/?portfolio=f722-std>. Accessed: 2021-02-04.

Mnih, V., Badia, A. P., Mirza, M., Graves, A., Lillicrap, T., Harley, T., Silver, D., and Kavukcuoglu, K. Asynchronous methods for deep reinforcement learning. In *International conference on machine learning*, pp. 1928–1937. PMLR, 2016.

Molchanov, A., Chen, T., Hönig, W., Preiss, J. A., Ayanian, N., and Sukhatme, G. S. Sim-to-(multi)-real: Transfer of low-level robust control policies to multiple quadrotors. *International Conference on Intelligent Robots and Systems*, 2019. URL <http://arxiv.org/abs/1903.04628>.

Mysore, S., Mabsout, B., Mancuso, R., and Saenko, K. Regularizing action policies for smooth control with reinforcement learning, 2020a.

Mysore, S., Mabsout, B., Saenko, K., and Mancuso, R. How to train your quadrotor: A framework for consistently smooth and responsive flight control via reinforcement learning, 2020b.

Pineau, J., Vincent-Lamarre, P., Sinha, K., Larivière, V., Beygelzimer, A., d'Alché Buc, F., Fox, E., and Larochelle, H. Improving reproducibility in machine learning research (a report from the neurips 2019 reproducibility program), 2020.

Raffin, A., Hill, A., Ernestus, M., Gleave, A., Kanervisto, A., and Dormann, N. Stable baselines3. <https://github.com/DLR-RM/stable-baselines3>, 2019.

Rusu, A. A., Colmenarejo, S. G., Gulcehre, C., Desjardins, G., Kirkpatrick, J., Pascanu, R., Mnih, V., Kavukcuoglu, K., and Hadsell, R. Policy distillation. *arXiv preprint arXiv:1511.06295*, 2015.

Sadeghi, F., Toshev, A., Jang, E., and Levine, S. Sim2Real view invariant visual servoing by recurrent control. *CoRR*, abs/1712.07642, 2017.

Schulman, J., Levine, S., Abbeel, P., Jordan, M., and Moritz, P. Trust region policy optimization. In Bach, F. and Blei, D. (eds.), *Proceedings of the 32nd International Conference on Machine Learning*, volume 37 of *Proceedings of Machine Learning Research*, pp. 1889–1897, Lille, France, 07–09 Jul 2015. PMLR.

Schulman, J., Wolski, F., Dhariwal, P., Radford, A., and Klimov, O. Proximal policy optimization algorithms. *CoRR*, abs/1707.06347, 2017.

Shen, H., Zhang, K., Hong, M., and Chen, T. Asynchronous advantage actor critic: Non-asymptotic analysis and linear speedup, 2020.

Sutton, R. S., McAllester, D. A., Singh, S. P., and Mansour, Y. Policy gradient methods for reinforcement learning with function approximation. In *Advances in neural information processing systems*, pp. 1057–1063, 2000.

Ullrich, K., Meeds, E., and Welling, M. Soft weight-sharing for neural network compression. *ArXiv*, abs/1702.04008, 2017.

Watkins, C. J. and Dayan, P. Q-learning. *Machine learning*, 8(3-4):279–292, 1992.

Zahavy, T., Xu, Z., Veeriah, V., Hessel, M., Oh, J., van Hasselt, H. P., Silver, D., and Singh, S. A self-tuning actor-critic algorithm. *Advances in Neural Information Processing Systems*, 33, 2020.

Zhang, A. X., Ballas, N., and Pineau, J. A dissection of overfitting and generalization in continuous reinforcement learning. *CoRR*, abs/1806.07937, 2018a.

Zhang, C., Vinyals, O., Munos, R., and Bengio, S. A study on overfitting in deep reinforcement learning. *CoRR*, abs/1804.06893, 2018b.

A. Toy Problem

A.1. Setup Details

The simple toy problem described in Section 3 of our main paper was designed to be one that is easily defined and easily solvable and was specifically designed such that a single-neuron actor would theoretically be able to solve the problem:

- **State space:** At time, t , the agent has target goal state, $g_t \in [-1, 1]$, and current internal state, $s_t \in [-1, 1]$. The agent however observes a simplified representation, i.e. the error between the current internal and target states. The state observation returned to the agent is a 1D error, $o_t = g_t - s_t$. Given that there are no complex dynamics in this system, this error can serve as a generalized state representation for which the ideal response is always the same.
- **Goal generation:** Goals g_t are procedurally generated by functions mapping an input ‘time’ signal to the range $[-1, 1]$. While only the simplex (noi) function is used in this work, other available goal generators include a constant goal or a step signal.
- **Action Space:** Actions are limited to the range of $a_t \in [-1, 1]$.
- **System Dynamics:** The response to action, a_t is computed as $s_{t+1} = \text{clip}(s_t + a_t, -1, 1)$.
- **Reward:** Reward is computed as $r_t = -|g_t - s_{t+1}|$.

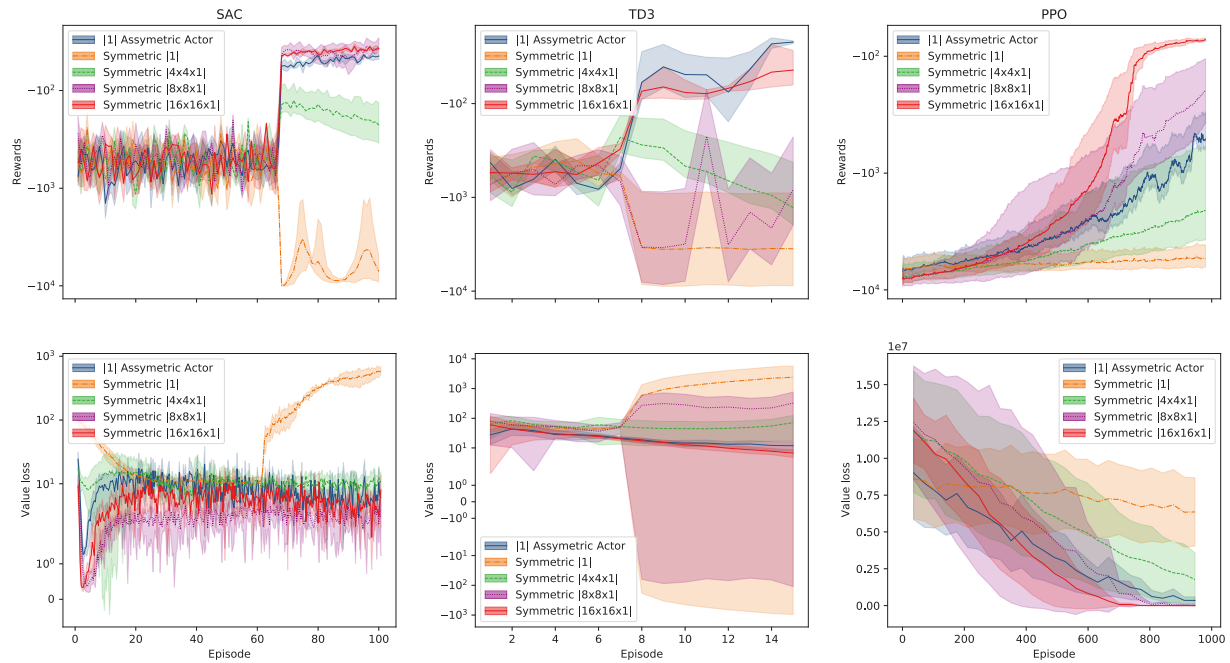


Figure A.1. Comparison of how rewards and value (critic) losses evolve during training on a simple toy-problem with SAC, TD3 and PPO. As with DDPG and TRPO (See Figure 1 of the main paper), results suggest a strong correlation between critic size and policy viability.

A.2. Additional Experiments

The training results presented in the main paper focus on DDPG (Lillicrap et al., 2016) and TRPO (Schulman et al., 2015) for illustrative purposes as those algorithms serve as the basis upon which more advanced algorithms have been built upon (with TD3 and SAC building upon DDPG and PPO building upon TRPO). The results we highlighted showed that maintaining actor-critic architectural symmetry did not allow small, 1-neuron actors to effectively learn to solve the toy problem outlined in Section 3 of our paper and further elaborated upon in Appendix A.1. We showed that it was however possible for 1-neuron actors to learn to solve the problem if we relaxed an implicit assumption on symmetry and instead paired smaller actors with larger critics (in this case, critics of size $[16, 16, 1]$). We observed that improvements in value

function estimation were typically followed by improvements in actor policies. Figure A.1 shows that these same trends, as noted on losses and rewards in Figure 1 in the main paper for DDPG and TRPO, can similarly be noted for TD3 (Fujimoto et al., 2018), SAC (Haarnoja et al., 2018) and PPO (Schulman et al., 2017).

Code for running experiments on this toy problem and corresponding README are included in the *Code/ToyProblem* folder of the zip-file containing this document. Training algorithms are based on OpenAI’s Spinning Up (Achiam, 2018) code-base.

B. Benchmarking Asymmetric Actors on OpenAI Gym — Extended Results

Table 1 of the main paper summarized experimental results of exploring the actor-size reduction benefits of actor-critic asymmetry. In this section, we provide data on the training rewards and losses for each of the algorithms tested, which include DDPG (Lillicrap et al., 2016), TD3 (Fujimoto et al., 2018), SAC (Haarnoja et al., 2018) and PPO (Schulman et al., 2017), on OpenAI Gym (Brockman et al., 2016) benchmarks. Five environments were tested: Pendulum-v0, Reacher-v2, Ant-v2, HalfCheetah-v2, Acrobot-v1. As with the toy problem, implementations for DDPG, TD3 and SAC are based on the OpenAI Spinning Up (Achiam, 2018) code-base. As discussed in the main paper, to preserve parity with published material, our PPO implementation is based on OpenAI’s Baselines (Dhariwal et al., 2017) code as it includes optimizations that are not included in the Spinning Up code-base (we note here that a similar note on the implementation specifics is made in the Spinning Up documentation). Experiments were run on a desktop computer running Ubuntu 18.04.5 LTS with an Intel Core i7-6850K CPU, Nvidia GeForce GTX 1080 Ti GPU, and 64GB RAM.

Code and corresponding README for running experiments with asymmetric actors and critics on registered OpenAI Gym is provided in the *Code/GeneralGym* folder of the zip-file containing this document.

B.1. Training Rewards

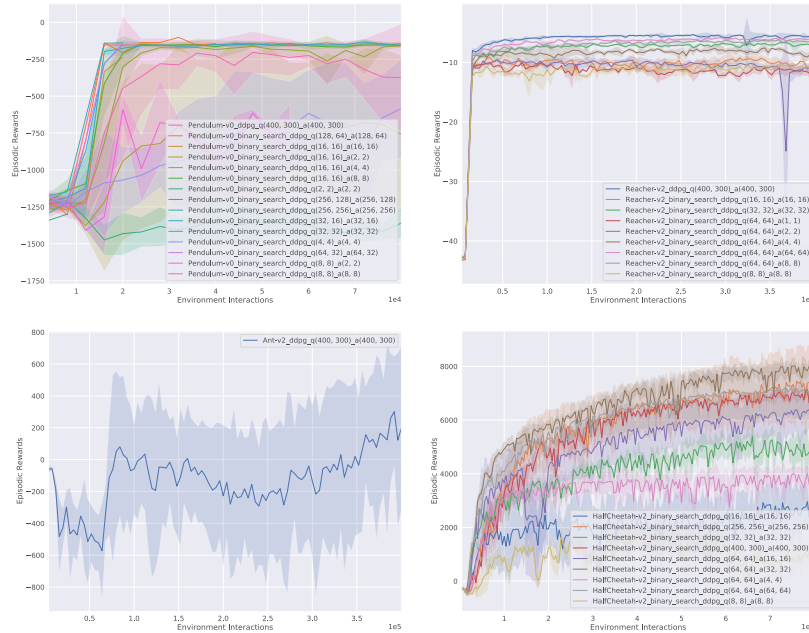


Figure B.1. Progress of training rewards for DDPG on Pendulum-v0, Reacher-v2, Ant-v2 and HalfCheetah-v2. Note DDPG’s failure to learn on the Ant-v2 environment

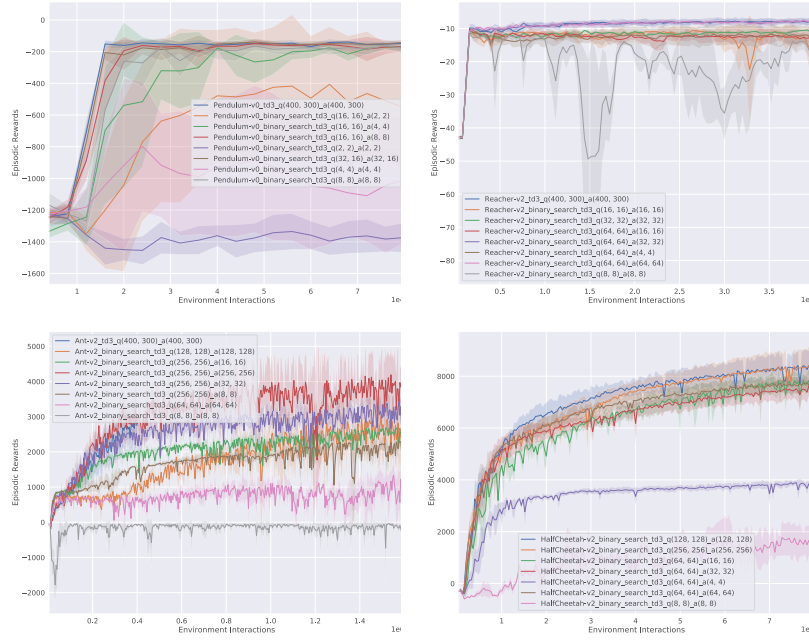


Figure B.2. Progress of training rewards for TD3 on Pendulum-v0, Reacher-v2, Ant-v2 and HalfCheetah-v2

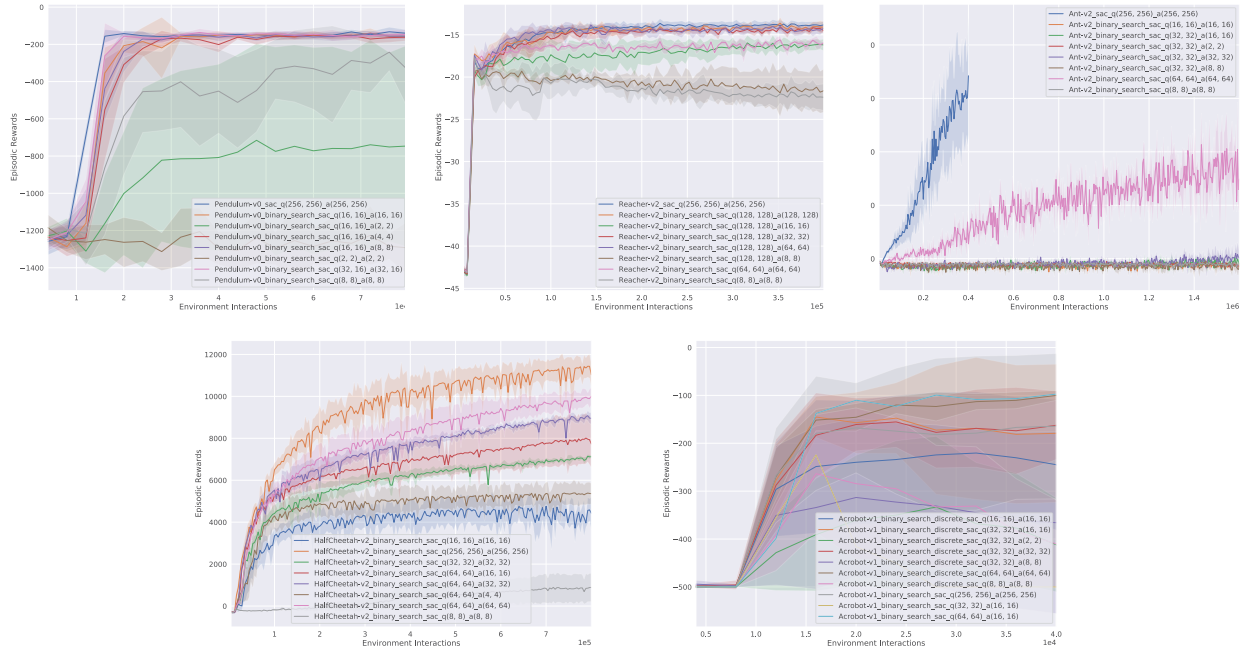


Figure B.3. Progress of training rewards for SAC on Pendulum-v0, Reacher-v2, Ant-v2, HalfCheetah-v2 and Acrobot-v1

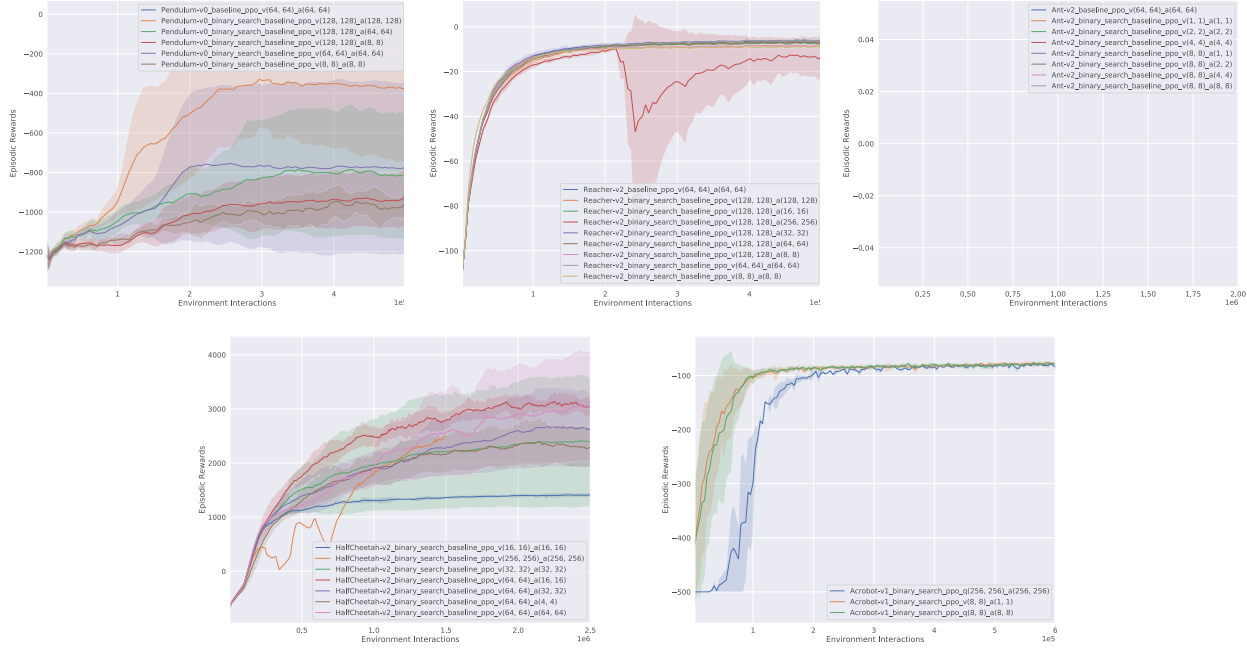


Figure B.4. Progress of training rewards for PPO on Pendulum-v0, Reacher-v2, Ant-v2, HalfCheetah-v2 and Acrobot-v1

B.2. Training Losses

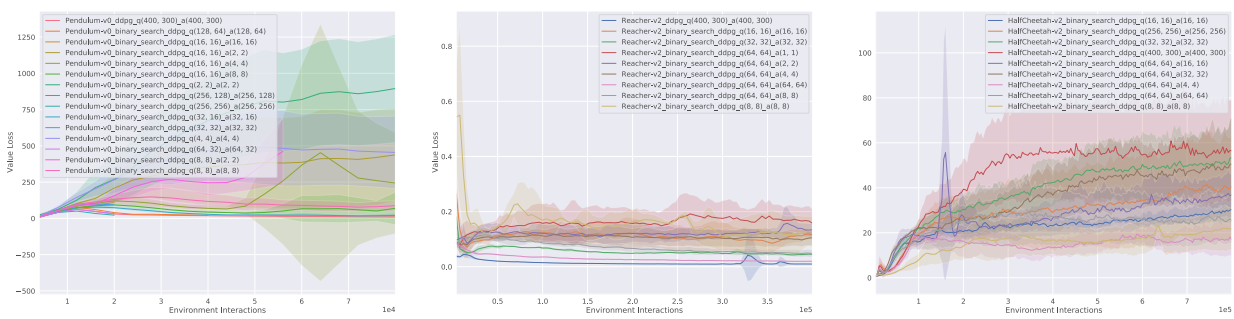


Figure B.5. Progress of value loss for the critic network for DDOG on Pendulum-v0, Reacher-v2 and HalfCheetah-v2. Note here that Ant-v2 is omitted due to DDPG failing to learn on this environment

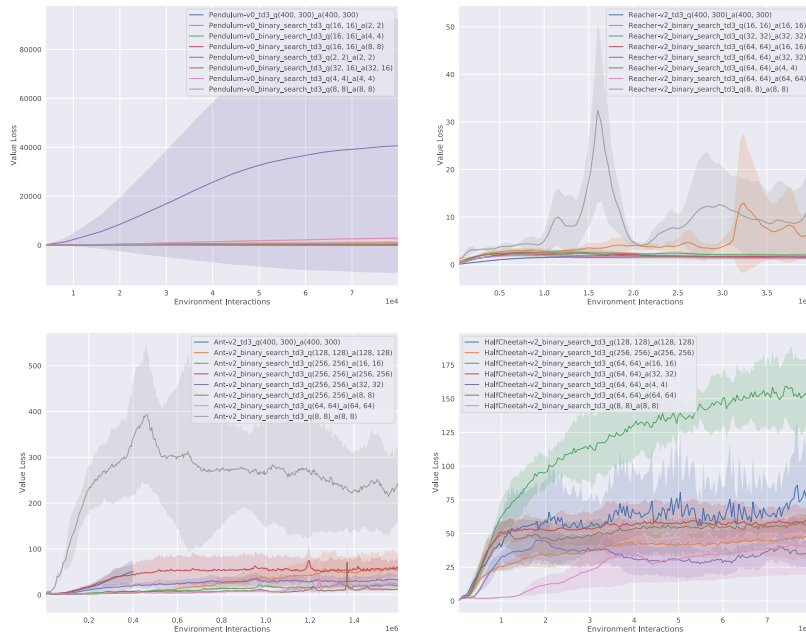


Figure B.6. Progress of average value loss for the critic networks for TD3 on Pendulum-v0, Reacher-v2, Ant-v2 and HalfCheetah-v2

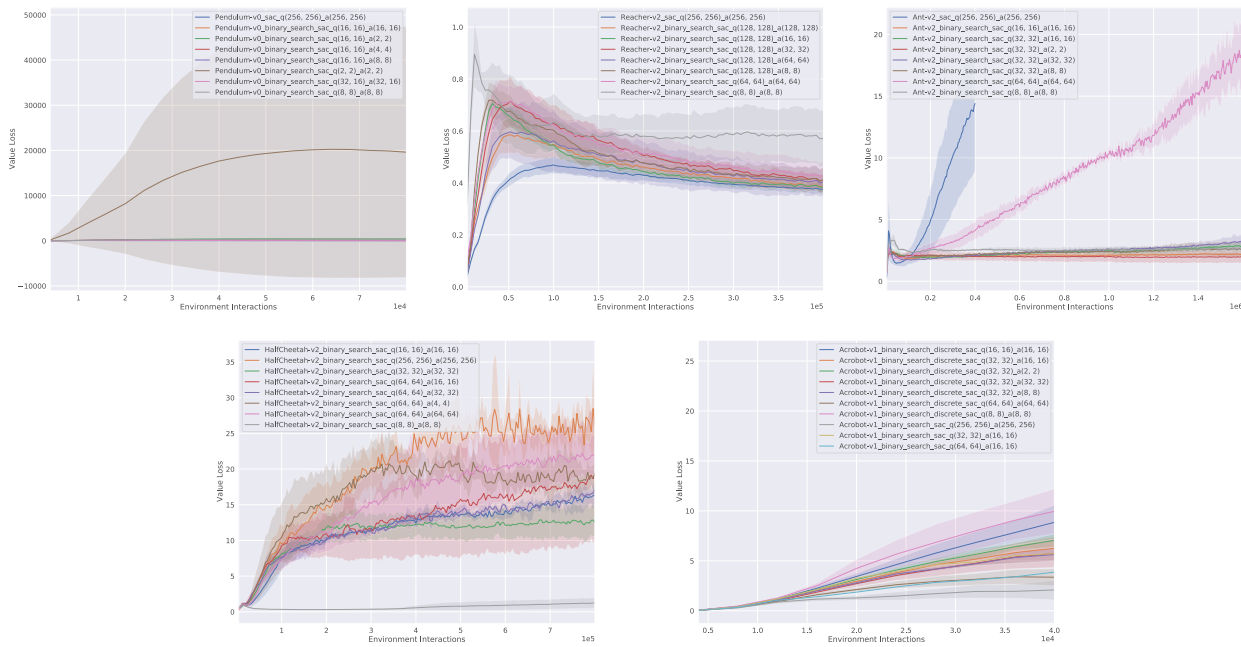


Figure B.7. Progress of average value loss for the critic networks for SAC on Pendulum-v0, Reacher-v2, Ant-v2, HalfCheetah-v2 and Acrobot-v1